摩擦学学报
TRIBOLOGY

金属摩擦接触界面的滑移测试及分析

李志杰，祁同晖，巴明森，覃文洁，赵振龙

Measurement and Analysis of Slips at Metal-to-Metal Frictional Contact Interfaces

LI Zhijie, QI Tonghui, BA Mingsen, QIN Wenjie, ZHAO Zhenlong

在线阅读 View online: https://doi.org/10.16078/j.tribology.2023136

李志杰, 祁同晖, 巴明森, 覃文洁, 赵振龙. 金属摩擦接触界面的滑移测试及分析[J]. 摩擦学学报（中英文）, 2024, 44(9): 1211−1218. LI Zhijie, QI Tonghui, BA Mingsen, QIN Wenjie, ZHAO Zhenlong. Measurement and Analysis of Slips at Metal-to-Metal Frictional Contact Interfaces[J]. Tribology, 2024, 44(9): 1211−1218. DOI: 10.16078/j.tribology.2023136

金属摩擦接触界面的滑移测试及分析

李志杰[1,2], 祁同晖[1,2], 巴明森[3], 覃文洁[3], 赵振龙[1,2*]
(1. 内燃机与动力系统全国重点实验室, 山东 潍坊 261000;
2. 潍柴动力股份有限公司, 山东 潍坊 261000;
3. 北京理工大学 机械与车辆学院, 北京 100081)

摘 要: 机械结构中紧固连接件受到切向载荷时接触界面上可能会发生微小的滑移, 在循环的切向载荷作用下, 这种微小的滑移可能是安定的, 也可能发生累积使得接触零件间发生较大的相对位移, 导致紧固连接失效. 本文中采用摩擦纳米发电机来测量接触界面间的滑移, 在搭建的滑移测试平台上对金属平面-平面接触的滑移累积进行了试验测试, 然后采用有限元法对这个过程进行数值模拟, 分析结果与测试结果接近. 对接触界面滑移累积和安定行为的机理进行剖析, 发现滑移安定时, 在第2个及以后循环载荷周期内, 界面上存在切向应力小于该处最大摩擦力的区域. 进一步通过数值模拟发现接触界面的滑移位移与载荷的大小、施加方式以及接触界面的变形有关.

关键词: 滑移; 摩擦接触; 摩擦纳米发电机; 有限元分析
中图分类号: TH117.1; TH131.2 **文献标志码:** A **文章编号:** 1004-0595(2024)09–1211–08

Measurement and Analysis of Slips at Metal-to-Metal Frictional Contact Interfaces

LI Zhijie[1,2], QI Tonghui[1,2], BA Mingsen[3], QIN Wenjie[3], ZHAO Zhenlong[1,2*]

(*1. State Key Laboratory of Engine and Powertrain System, Shandong Weifang 261000, China;*
2. Weichai Power Cooperation Limited, Shandong Weifang 261000, China;
3. School of Mechanical and Vehicular Engineering, Beijing Institute of Technology, Beijing 100081, China)

Abstract: Lots of components in mechanical systems are connected by friction contacts, such as bolts joints, shafts and bushings, etc. When they are subjected to tangential loads, small slips may occur at the friction contact interfaces. Under multiple cyclic tangential loads, the small slips may just occur at the early stages and cease after some cycles, reaching a shakedown state. Sometimes the slips may be cumulative and cause a significant relative displacement between the contact parts, leading to failure of the connections. But this micro slip is difficult to measure directly, and people often can only measure the relative displacement between the contact parts. In this article, a triboelectric nanogenerator, which was of vertical contact-separation type was used to measure the slip in a metal flat-on-flat contact in the testing platform. In the triboelectric nanogenerator fabricated in this study, two triboelectric layers were fixed on the two test pieces separately at the contact interface and were in contact initially, and the open-circuit voltage generated by the separation of the triboelectric layers could be adopted to characterize the relative slip displacement of the contact surfaces, because the magnitude of the open-circuit voltage was proportional to the separation displacement of the triboelectric layers, which was the same as the slip displacement of the contact surfaces. The slip testing platform established in this study

Received 14 July 2023, revised 18 September 2023, accepted 19 September 2023, available online 2 April 2024.
*Corresponding author. E-mail: zhaozl@weichai.com, Tel: +86-15318939615.
This project was supported by the Science Fund of State Key Laboratory of Engine and Powertrain System (SKLER-202111).
内燃机与动力系统全国重点试验室开放基金项目(SKLER -202111)资助.

included the vibration exciter, the upper test piece, the lower test piece, the force application piece, the excitation force sensor, the triboelectric nanogenerator, the power amplifier, the Keithley 6514 electrometer and the 6500 data acquisition system. The linear relationship between the open circuit voltage of the triboelectric nanogenerator and the separation displacement of the triboelectric layers was obtained by calibration. Then, the accumulation of slips in the metal flat-on-flat contact were tested using the slip testing platform, in which the upper test piece subjected to the uniform normal pressure generated by the force application piece was in contact with the lower test piece, and the vibration exciter was pressed on the left side of the upper test piece to apply cyclic tangential loads. When the upper test piece slipped relative to the lower test piece, the triboelectric nanogenerator would generate an electrical signal due to separation of the triboelectric layers, which was collected by the 6514 electrometer and the 6500 data acquisition system and converted to the slip displacement of the upper test piece. Then, the finite element model of the flat-on-flat contact configuration in the experiment was developed and the dynamic analysis was implemented to simulate this process. The simulation results were in good agreement with the experimental results. Based on the finite element dynamic analysis, the mechanisms of accumulation and shakedown behaviors of slips at contact interfaces were analyzed. It was found that there existed an area on the interface where the tangential stress was less than the maximum friction stress during the second and subsequent load cycles when the slip was shakedown. Further numerical simulation results showed that the slip displacement was related to the magnitude and form of the load, as well as the deformation at the contact interface. As the normal load increased, the tangential load required for the same slip displacement of the upper specimen did not increase proportionally. This was because the increase in normal load leads to a decrease in the sticking area at both ends of the contact surface. By using the decreasing normal load along the surface of the upper specimen with the maximum value on the side where the tangential force was applied, the edge areas of the contact surfaces could be more closely fitted and slip displacement could be reduced.

Key words: slip; frictional contact; triboelectric nanogenerator; finite element analysis

在机械系统中有许多依靠摩擦接触来实现紧固连接的结构，当受到循环的切向载荷时，零件之间的接触界面上会产生微小的切向滑移，这种滑移累积到一定程度时，会使零件间发生宏观的滑动[1]，导致紧固连接的失效，如螺纹的松动[2-5]严重时会引发重大的安全事故.

针对金属摩擦接触的滑移行为，国内外学者在理论研究、数值模拟和试验分析方面开展了大量工作. 比如在理论研究方面，Mindlin[6]针对轴线相互平行的圆柱体接触，提出了局部滑移问题的理论求解方法，将滑移区和黏着区切向力叠加，得出了切向力与接触面黏着区半径的关系式. Porisky[7]针对接触面椭圆分布的切向力求解出了接触面间部分滑移的切向位移. 许多研究认为滑移累积是造成摩擦紧固连接结构松动的主要原因，为了防止这种松动，接触界面的滑移就需要是安定的，因此不少学者对滑移的安定条件进行了理论分析，认为对于非耦合接触系统来说存在1个安定极限，而对于耦合接触系统来说则存在1个上限条件和1个下限条件，作用于系统上的切向载荷幅值小于下限时系统是安定的，大于上限时系统不存在安定状态[8-13].

在数值模拟方面，Ligier等[14]指出发动机中轴承和连杆之间产生的微小滑移累积会导致二者发生相对旋转，提出了产生初始微滑移的临界载荷，并指出决定微滑移位移的关键参数是摩擦系数和切向刚度. 还有许多学者针对螺纹连接接触面的滑移及其导致的松动进行了探究，如Pai和Hess[15-16]提出了螺纹啮合区不同接触状态下的4种不同松动过程，通过建立三维有限元模型，对4种不同松动过程的螺纹啮合面的完全滑移和局部滑移进行了分析研究，提出了影响紧固件接触面滑移的影响因素.

在试验研究方面，美国内华达大学机械工程系Jiang等[17-18]搭建了螺栓松动检测试验装置，结合有限元模拟，提出螺栓与螺母的螺纹啮合面发生了微小的滑移会导致螺栓发生松动，并对其微小滑移进行了定性分析，后又设计了新的试验测试装置，提出螺栓在动载荷作用下的松动过程可分为初期松动及后期加速松动2个阶段，前期松动螺母不发生转动，后期松动才发生转动，并通过测试螺栓和螺母的相对旋转角度来得到二者啮合面的滑移位移[19]. 但是该试验只能测得接触界面滑移后期滑移状况，对其前期滑移情况无法测量.

上述研究中，理论研究的对象一般都是简化的理想模型，针对实际结构的数值模拟重点考察的是接触滑移对结构性能的影响，没有涉及滑移安定的问题. 试验测试大多是测量接触物体之间的位移，而并不能

直接测量接触界面上某个位置的滑移位移. 2012年, 佐治亚理工学院的王中林教授首次提出了摩擦纳米发电机(Triboelectric nanogenerator, TENG)的概念, 其可以通过2种不同材料的接触或摩擦产生电荷并发生电荷的流动, 将机械能转化为电能, 而其输出的电信号(电压、电流)可以用来分析相应的机械输入信号, 可用作自驱动(主动式)传感器[20–23]. 本文中提出采用摩擦纳米发电机来直接测量接触界面的滑移位移, 并运用于金属平面-平面接触的微动滑移测试中, 进一步运用有限元法对其进行数值模拟, 分析不同滑移行为产生的原因以及法向载荷的大小及形式对金属平面-平面接触滑移位移的影响.

1　摩擦滑移行为

对于相互接触的弹性体, 设接触面上一点的法向应力和切向应力分别为σ_{n}和σ_{t}, 法向和切向位移为u_{n}和u_{t}, 根据库伦摩擦定律, 接触面法线方向上应满足

$$\sigma_{\mathrm{n}} \geqslant 0,\ u_{\mathrm{n}} - g \leqslant 0,\ \sigma_{\mathrm{n}}(u_{\mathrm{n}} - g) = 0 \tag{1}$$

切线方向上应满足

$$\begin{aligned} &|\sigma_{\mathrm{t}}| \leqslant \mu\sigma_{\mathrm{n}} \\ &|\sigma_{\mathrm{t}}| < \mu\sigma_{\mathrm{n}} \Rightarrow \dot{u}_{\mathrm{t}} = 0 \quad (\text{Sticking}) \\ &|\sigma_{\mathrm{t}}| = \mu\sigma_{\mathrm{n}} \Rightarrow \dot{u}_{\mathrm{t}} = -\lambda\sigma_{\mathrm{t}}, \lambda \geqslant 0 \quad (\text{Slipping}) \end{aligned} \tag{2}$$

式中, μ 是摩擦系数, $\dot{u}_{\mathrm{t}}$为切向相对速度, g为接触面间的初始间隙, λ为不为负的系数.

在变化的载荷作用下, 接触界面的微滑可能发生累积, 产生棘轮现象, 即在每个微动循环后切向位移都会有所增加, 满足式(3), 结构的滑移将发生累积导致宏观的滑动.

$$\oint_{\text{cycle}} \dot{u}_{\mathrm{t}}(x,t)\mathrm{d}t = R\boldsymbol{\tau},\ R \neq 0 \tag{3}$$

式中, x代表接触面上一点的位置, t是时间, R是切向滑移位移增量, $\boldsymbol{\tau}$是切向向量[1].

接触界面的微滑也可能是安定的, 如果滑移只存在于前几个微动循环, 后续循环中的滑移是纯弹性或可逆的, 这种情况称为安定, 切向位移趋于1个有限的定值, 即[1]

$$\lim_{t\to\infty} u_{\mathrm{t}}(x,t) = u_{\mathrm{t}}^{\infty}(x) \tag{4}$$

2　试验装置及测试结果

2.1　试验装置

本文中使用的试验装置如图1(a)所示, 包括施力件、上试件、下试件、功率放大器、激振器、激振力传感器、预紧力传感器, 吉时利(Keithley) 6514型静电计、6500数据采集系统和摩擦纳米发电机, 其中上试件受到施力件产生的均匀压力与下试件接触. 将摩擦纳米发电机的2个摩擦层分别与上、下试件在接触面的中点处固定在一起, 并使其相对贴合, 如图1(b)所示. 通过激振器对上试件施加循环激振力, 当上、下试件发生相对滑移时, 摩擦纳米发电机的2个摩擦层发生分离即可产生电信号并被静电计和数据采集系统记录.

2.2　摩擦纳米发电机的测试原理及制作

摩擦纳米发电机主要有4种工作模式, 分别是垂直接触-分离模式、水平滑动模式、单电极模式和独立层模式, 本文试验中使用的是垂直接触-分离模式, 2个摩擦层分别为导体和电介质, 其中的导体既是电极也是摩擦层, 其原理如图2所示.

图2中电介质摩擦层的厚度为d, 两摩擦层分开的距离记为$x(t)$, 面积记为S. 假设摩擦层的尺寸远大于d+$x(t)$, 可以认为是无限大平板, 电荷均匀地分布在其表面. 当2个摩擦层接触后其内表面将带上密度相等、符号相反的静电荷, 记为ρ. 当2个摩擦层分开时, 2个电极之间会产生电荷的转移, 设转移的电荷量为Q,

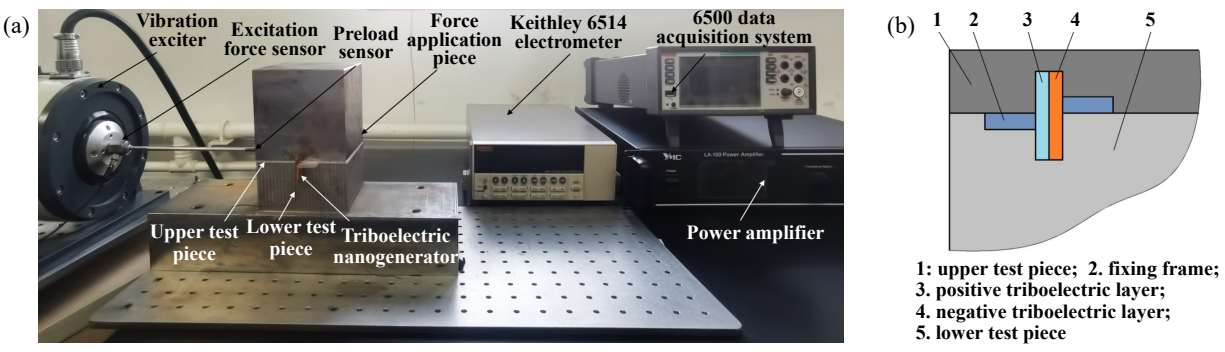

Fig. 1　Test bench: (a) test bench; (b) triboelectric nanogenerator

图 1　试验装置: (a)试验装置; (b)摩擦纳米发电机

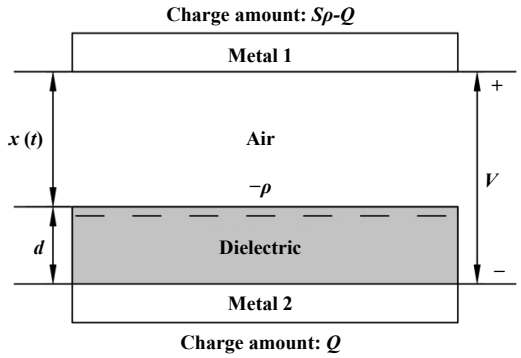

Fig. 2 Principle of the triboelectric Nanogenerator

图 2 摩擦纳米发电机的工作原理

则电介质内的电场强度为[24]

$$E = \frac{-Q}{S\varepsilon_0\varepsilon_r} \tag{5}$$

式中，ε_r为电介质的相对介电常数，ε_0是真空介电常数.

在间隙中，电场分布为

$$E_a = \frac{-Q/S + \rho}{\varepsilon_0} \tag{6}$$

两金属电极之间的电压为

$$V = Ed + E_a x(t) = -\frac{Q}{S\varepsilon_0}\left[\frac{d}{\varepsilon_r} + x(t)\right] + \frac{\rho x(t)}{\varepsilon_0} \tag{7}$$

开路状态时，两电极之间没有电荷转移，即Q=0，此时两电极之间电压为

$$V_{OC} = \frac{\rho x(t)}{\varepsilon_0} \tag{8}$$

从式(8)中可以看出开路电压的大小与摩擦层分离的距离线性相关，因此可以利用此特性做自供电位移传感器，且不需要外接电源即可用来测量滑移距离.

在本文中的试验测试装置中安装的摩擦纳米发电机的结构组成如图3所示，每个摩擦层的尺寸为25 mm×10 mm，其中1个摩擦层采用铜膜制成(同时作为电极)，另一个摩擦层的材料为PTFE，其电极材料为金属铜，二者都粘接在厚度为2 mm的亚克力基底上. 从2个电极引出导线，接入吉时利6514型静电计，静电计与6500数据采集系统相连.

2.3 测试标定

使摩擦纳米发电机的2个摩擦层每次分离的距离为0.8 mm，得到的开路电压如图4所示. 从图4中可以看出当2个摩擦层分离0.8 mm时产生的平均开路电压为2.65 V，则由公式(8)可得测得的开路电压V/V与分离距离x/mm的关系为

$$V = 3.31x \tag{9}$$

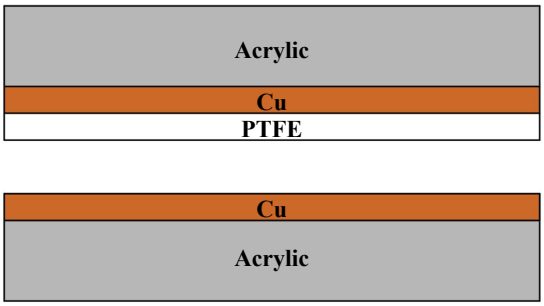

Fig. 3 Schematic diagram of the triboelectric Nanogenerator structure

图 3 摩擦纳米发电机结构示意图

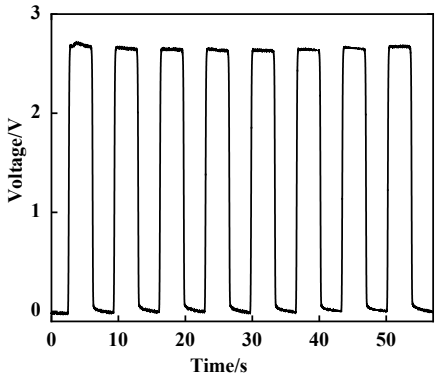

Fig. 4 Open circuit voltage of the triboelectric nanogenerator with a separation distance of 0.8 mm

图 4 分离距离为0.8 mm时摩擦纳米发电机的开路电压

2.4 测试结果

当上下试件的材料分别为ZL111和42CrMo时，试验测得其摩擦系数为0.182. 在上试件的左端中点处施加预压力及往复激振力，使其受到的激振力为脉冲力，当其幅值达到14.88 N时，脉冲力幅值大于界面的总摩擦力14.00 N，上试件开始发生滑移，然后激振力开始下降，上试件逐渐停止滑移，如图5(a)所示. 由摩擦纳米发电机测得的开路电压按式(9)可计算得到这个过程的滑移位移，如图5(b)所示，在初始滑移阶段的5个循环载荷内平均滑移位移为8.49 μm.

3 仿真及结果分析

3.1 有限元模型

从试验测试结果可以看出，上试件在每个切向激励载荷循环下的滑移位移很小，只有几微米，难以直观地观察到，为此本文中利用有限元分析软件Abaqus对这个过程进行了数值模拟. 分别建立施力件、上试件和下试件的二维模型，并将其装配在一起，如图6(a)所示. 其中上试件尺寸为100 mm×2 mm，下试件尺寸为100 mm×4 mm，二者的材料参数列于表1中. 为简化

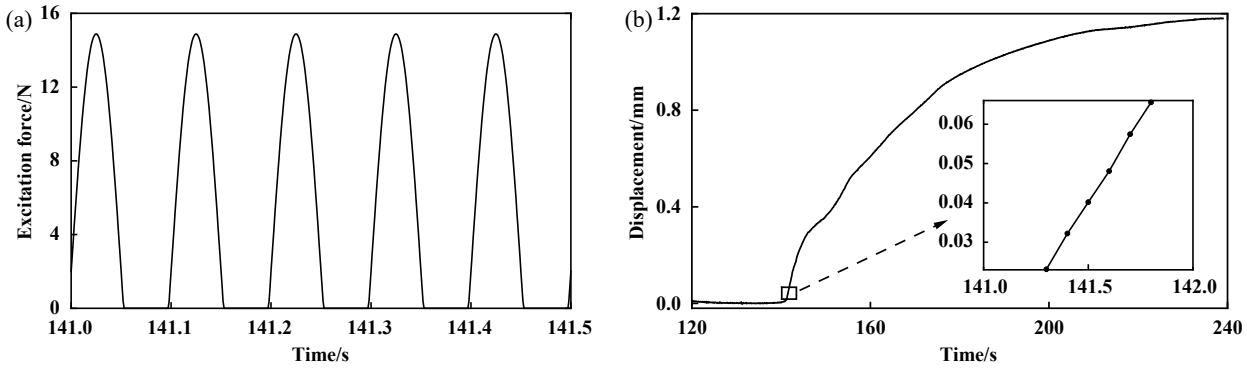

Fig. 5　Test results of slip displacement: (a) excitation force; (b) slip displacement

图 5　滑移测试结果: (a)激振力; (b)滑移位移

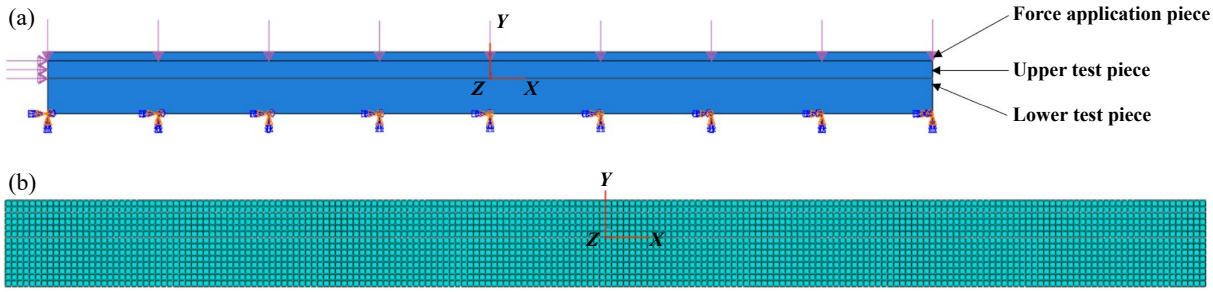

Fig. 6　Finite element model: (a) boundary condition; (b) mesh model

图 6　有限元模型: (a)边界条件; (b)网格模型

模型将施力件的尺寸设置为100 mm×1 mm, 通过设置合适的密度使其质量与原立方体的质量相等. 将下试件的下底面固定, 在上试件的上表面施加均布法向载荷, 左侧施加循环切向载荷. 在上下试件之间施加摩擦接触, 摩擦系数由试验测得为0.182. 采用平面应变单元进行网格划分, 单元尺寸为0.50 mm, 网格模型如图6(b)所示.

表 1　材料参数

Table 1　Material parameters

Material	Elastic modulus/GPa	Poisson's ratio	Density/(kg/m^3)
ZL111	70	0.34	2 690
42CrMo	212	0.28	7 850

3.2　滑移累积的仿真结果

将试验中上试件发生滑移时测得的循环切向力施加在模型上试件中, 经动力学分析后得到5个循环载荷下接触面中间节点的滑移曲线随时间的变化如图7所示, 从图7可得该结点的平均滑移距离为8.65 μm, 与试验测试结果8.49 μm的平均滑移距离十分接近.

在开始发生滑移时刻上试件接触面上各结点的接触法向应力如图8(a)所示, 可以看出大部分区域节点的法向应力分布较均匀, 左侧节点处由于施加切向

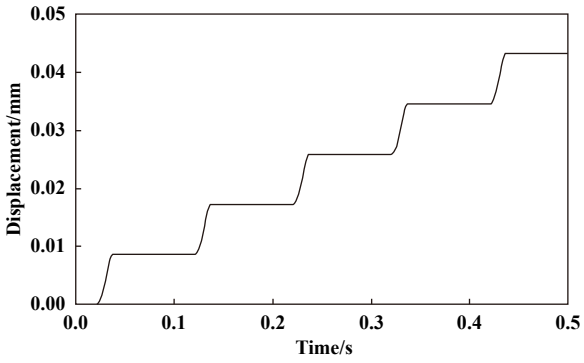

Fig. 7　Simulation results of slip displacement at the middle node on the contact surface of the upper specimen

图 7　上试件接触面中间结点的滑移位移仿真结果

载荷会引起一部分接触面翘曲分离, 从而导致接触法向应力为0. 此时接触面上各节点的接触切向应力如图8(b)所示, 界面上各点的切向应力等于法向应力与摩擦系数(μ)的乘积, 即$|\sigma_t| = \sigma_n \times \mu$, 因此整个界面上都发生了滑移. 此后在每个载荷循环中切向激励载荷达到峰值时界面上各结点的接触应力都满足这个条件, 也就是在每个载荷循环中都会产生新的滑移位移, 界面的滑移发生了累积.

3.3　滑移安定结果及分析

保持法向载荷不变, 逐渐减小切向力, 当切向力

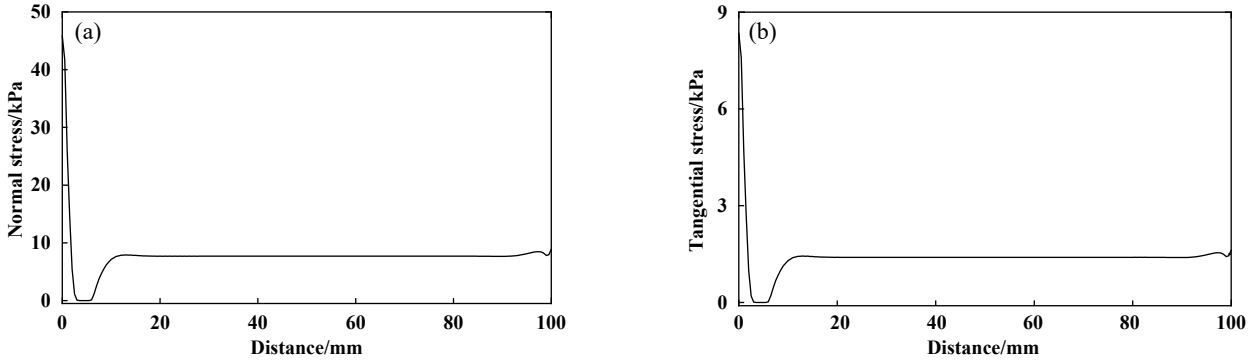

Fig. 8 Contact stress on the contact surface of the specimen at the moment of slipping: (a) normal stress; (b) tangential stress

图 8 滑移时刻上试件接触表面各点的接触应力:(a)法向应力;(b)切向应力

减小到14.03 N时,滑移出现安定. 在第1个循环切向载荷作用下,切向力达到峰值时刻接触界面的滑移状态如图9(a)所示,绿色部分代表滑移区域,红色代表黏着区域,可以看出上试件在第1个切向载荷循环内的发生了整体滑移,在第2个和第3个切向载荷循环内的相同时刻接触界面均存在黏着区域,没有发生整体滑移,如图9(b)和(c)所示.

考察图9中右侧的红色黏着区域内一结点的切向应力随时间变化,如图10所示,可以看出在第1周期循环载荷作用下,切向应力存在一段水平曲线,这时$|\sigma_t| = \sigma_n \times \mu$,在这段时间内该点发生了滑移;而在以后的循环载荷作用下,切向应力始终满足$|\sigma_t| < \sigma_n \times \mu$,该点不再产生新的滑移,处于滑移安定状态.

从图9中还可以看出,随着载荷循环的增加,滑移时刻上、下试件接触界面之间黏着区域逐渐扩展. 考察右端红色黏着区域处一结点的切向速度随时间变化,如图11所示,可以看出在第1周期内上试件的滑移速度较大,达到最大速度之后速度减小并变为负值,而后在接下来的载荷循环中该结点的最大正向速度明显减小,只有正负交替变化的弹性变形,此时滑移达到安定状态.

4 不同的法向载荷对滑移行为的影响分析

4.1 增大法向载荷

对于滑移累积的情况,保持施加的切向载荷的预压力不变,当施加的法向载荷增加到原来的10倍时,仿真得到在上试件达到相同的滑移距离时所需要的切向循环载荷幅值为143.0 N,其值略小于原来切向载荷幅值的10倍. 当法向载荷增加到原来的100倍时,上试件达到相同的滑移距离时所需要的切向循环载荷幅值为1 410 N,同样小于原来切向载荷幅值的100倍. 当法向载荷增加到原来的1 000倍时,上试件达到相同的滑移距离时所需要的切向循环载荷幅值为14 034 N,也小于原来切向载荷幅值的1 000倍.

可以看出当法向载荷成倍增加时,达到同样滑移距离所需要的切向力并不会同比例增加,这是因为当法向载荷增加时会导致两端的接触区域在没有施加切向载荷时就发生了部分滑移,如图12所示,整个接触面上黏着区域的面积减小,使得滑移相同距离所需要的切向力幅值也随之减小.

4.2 改变法向载荷形式后的滑移位移

从图8可以看出,由于切向载荷的作用,接触界面

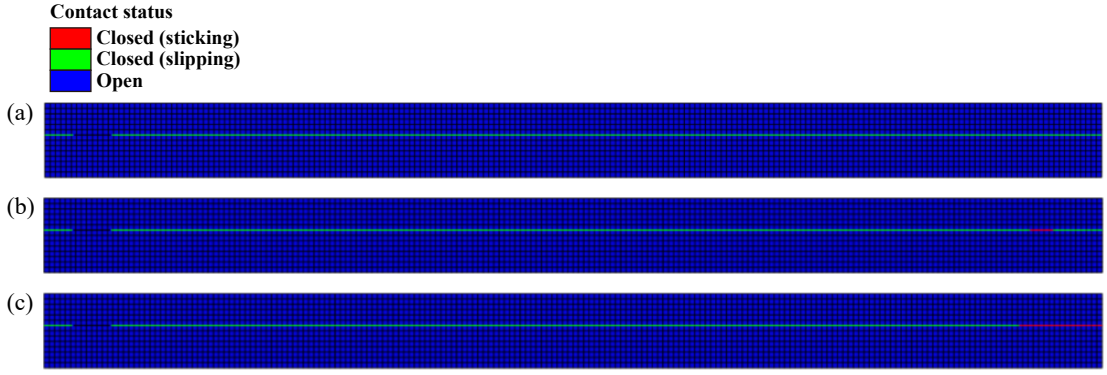

Fig. 9 Contact statuses under different load cycles: (a) first load cycle; (b) second load cycle; (c) third load cycle

图 9 不同载荷循环下接触界面的接触状态:(a)第1个载荷循环;(b)第2个载荷循环;(c)第3个载荷循环

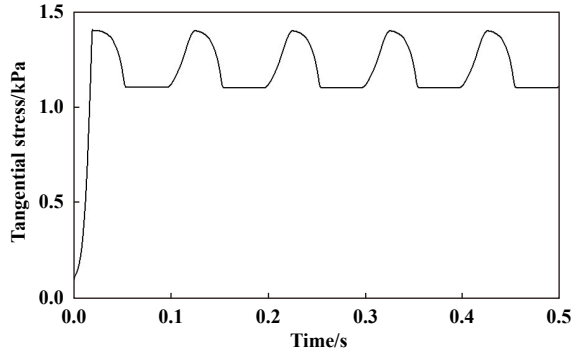

Fig. 10　Change of the tangential stress at one node in the sticking zone with time

图 10　黏着区内结点的切向应力随时间的变化

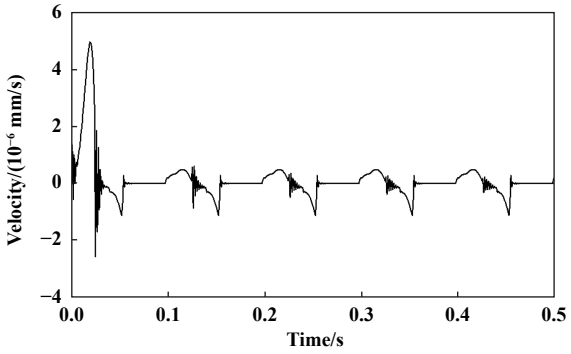

Fig. 11　Tangential velocity at one node in the sticking zone

图 11　黏着区内结点的切向速度随时间的变化

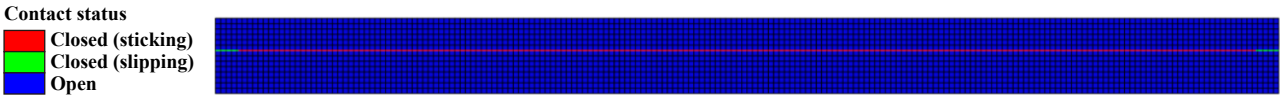

Fig. 12　The initial contact status at the contact interface when increasing the normal load

图 12　增大法向载荷时接触界面的初始接触状态

的左侧会有一小部分接触面发生翘曲分离，为此本文中设计了1种从大逐渐减小到零但总值为原法向载荷1 000倍的递减法向载荷，如图13所示，切向力也保持为14 034 N. 仿真得到上试件的滑移位移如图14所示，可得上试件接触面上中间结点的平均滑移位移为7.16 μm，与均布法向载荷作用下该结点的平均滑移位移8.49 μm相比，递减法向载荷作用下产生的平均滑移位移较小.

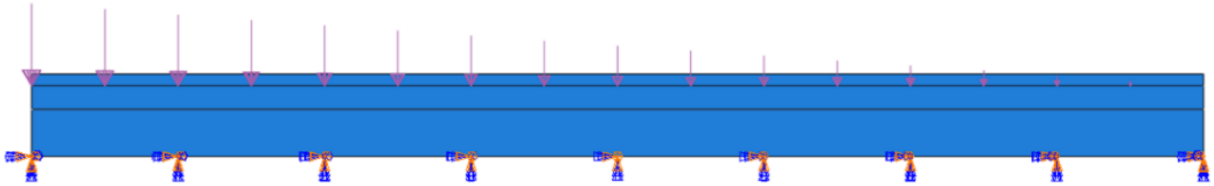

Fig. 13　Decreasing normal load distribution

图 13　递减的法向载荷分布

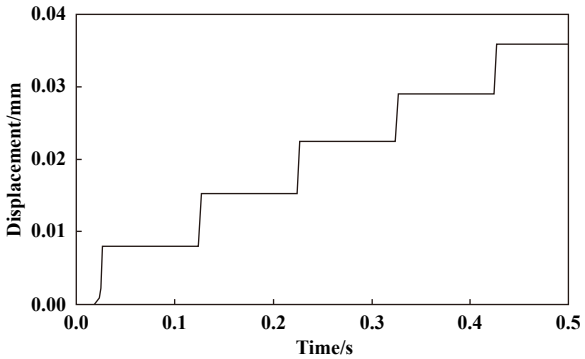

Fig. 14　Slip displacements of the middle node on the contact surface of the upper specimen under decreasing normal load

图 14　递减分布的法向载荷下上试件接触面中间结点的滑移位移

5　结论

本文中采用摩擦纳米发电机来测量金属平面-平面摩擦接触的滑移位移，并通过数值模拟分析了接触界面滑移安定及累积的原因及法向载荷的影响，得出了以下结论：

a. 采用摩擦纳米发电机可直接准确地测量接触界面上微米量级的滑移位移.

b. 当接触物体上受到峰值大于界面的总摩擦力的切向循环载荷时，接触界面可能发生滑移累积或安定. 发生滑移安定时，在第2个及以后循环载荷周期内，界面上存在切向应力小于该处最大摩擦力的区域.

c. 通过对金属平面-平面接触的数值模拟发现接触界面的滑移位移与载荷的大小、施加方式以及接触界面的变形有关. 随着法向载荷的增大，上试件发生相同的滑移距离所需要的切向力并不会同比例增大，这是法向载荷增大会导致接触边缘区域黏着面积减小的缘故，而采用在施加切向力的一侧法向力最大的

递减法向载荷，可以使得边缘接触区域更加贴合，减小滑移位移.

参 考 文 献

[1] Antoni N, Nguyen Q S, Ligier J L, et al. On the cumulative microslip phenomenon[J]. European Journal of Mechanics - A/Solids, 2007, 26(4): 626–646. doi: 10.1016/j.euromechsol.2006.09.004.

[2] Gong Hao, Liu Jianhua, Feng Huihua, et al. Concept of radial slippage propagation triggering self-loosening and optimisation design of novel anti-loosening structures[J]. Friction, 2023, 11(6): 865–880. doi: 10.1007/s40544-022-0618-5.

[3] Gong Hao, Liu Jianhua, Ding Xiaoyu. Study on local slippage accumulation between thread contact surfaces and novel anti-loosening thread designs under transversal vibration[J]. Tribology International, 2021, 153: 106558. doi: 10.1016/j.triboint.2020.106558.

[4] Izumi S, Kimura M, Sakai S. Small loosening of bolt-nut fastener due to micro bearing-surface slip: a finite element method study[J]. Journal of Solid Mechanics and Materials Engineering, 2007, 1(11): 1374–1384. doi: 10.1299/jmmp.1.1374.

[5] Dinger G, Friedrich C. Avoiding self-loosening failure of bolted joints with numerical assessment of local contact state[J]. Engineering Failure Analysis, 2011, 18(8): 2188–2200. doi: 10.1016/j.engfailanal.2011.07.012.

[6] Mindlin R D. Compliance of elastic bodies in contact[J]. Journal of Applied Mechanics, 1949, 16(3): 259–268. doi: 10.1115/1.4009973.

[7] Poritsky H. Stresses and deflections of cylindrical bodies in contact with application to contact of gears and of locomotive wheels[J]. Journal of Applied Mechanics, 1950, 17(2): 191–201. doi: 10.1115/1.4010099.

[8] Klarbring A, Barber J R, Spagnoli A, et al. Shakedown of discrete systems involving plasticity and friction[J]. European Journal of Mechanics - A/Solids, 2017, 64: 160–164. doi: 10.1016/j.euromechsol.2017.02.006.

[9] Cwiekala N, Barber J R, Hills D A. Frictional shakedown of a coupled continuous contact[J]. International Journal of Solids and Structures, 2023, 274: 112293. doi: 10.1016/j.ijsolstr.2023.112293.

[10] Ponter A R S. Shakedown limit theorems for frictional contact on a linear elastic body[J]. European Journal of Mechanics - A/Solids, 2016, 60: 17–27. doi: 10.1016/j.euromechsol.2016.05.003.

[11] Andersson L E, Barber J R, Ponter A R S. Existence and uniqueness of attractors in frictional systems with uncoupled tangential displacements and normal tractions[J]. International Journal of Solids and Structures, 2014, 51(21-22): 3710–3714. doi: 10.1016/j.ijsolstr.2014.07.004.

[12] Ahn Y J, Klarbring A, Spagnoli A, et al. Shakedown in frictional contact of discrete elastic systems: a review[J]. International Journal of Solids and Structures, 2022, 241: 111470. doi: 10.1016/j.ijsolstr.2022.111470.

[13] Spagnoli A, Terzano M, Barber J R, et al. Non-linear programming in shakedown analysis with plasticity and friction[J]. Journal of the Mechanics and Physics of Solids, 2017, 104: 71–83. doi: 10.1016/j.jmps.2017.04.006.

[14] Ligier J L, Antoni N. Cumulative microslip in conrod big end bearing system[C]//Proceedings of ASME 2006 Internal Combustion Engine Division Spring Technical Conference, 2006, Aachen, Germany. doi:10.1115/ICES2006-1357.

[15] Pai N G, Hess D P. Experimental study of loosening of threaded fasteners due to dynamic shear loads[J]. Journal of Sound and Vibration, 2002, 253(3): 585–602. doi: 10.1006/jsvi.2001.4006.

[16] Pai N G, Hess D P. Three-dimensional finite element analysis of threaded fastener loosening due to dynamic shear load[J]. Engineering Failure Analysis, 2002, 9(4): 383–402. doi: 10.1016/S1350-6307(01)00024-3.

[17] Jiang Y Y, Zhang M, Lee C H. A study of early stage self-loosening of bolted joints[J]. Journal of Mechanical Design, 2003, 125(3): 518–526. doi: 10.1115/1.1586936.

[18] Zhang M, Jiang Y Y, Lee C H. Finite element modeling of self-loosening of bolted joints[J]. Journal of Mechanical Design, 2007, 129(2): 218–226. doi: 10.1115/1.2406092.

[19] Jiang Y Y, Zhang M, Park T W, et al. An experimental study of self-loosening of bolted joints[J]. Journal of Mechanical Design, 2004, 126(5): 925–931. doi: 10.1115/1.1767814.

[20] Wang Zhonglin. On Maxwell's displacement current for energy and sensors: the origin of nanogenerators[J]. Materials Today, 2017, 20(2): 74–82. doi: 10.1016/j.mattod.2016.12.001.

[21] Lei Wenqian, Lu Shan, Wang Qi, et al. A method of measuring weak-charge of self-powered sensors based on triboelectric nanogenerator[J]. Nano Energy, 2022, 95: 106997. doi: 10.1016/j.nanoen.2022.106997.

[22] Chen Longping, Yuan Kang, Chen Shiyang, et al. Triboelectric nanogenerator sensors for intelligent steering wheel aiming at automated driving[J]. Nano Energy, 2023, 113: 108575. doi: 10.1016/j.nanoen.2023.108575.

[23] Han Qinkai, Ding Zhuang, Qin Zhaoye, et al. A triboelectric rolling ball bearing with self-powering and self-sensing capabilities[J]. Nano Energy, 2020, 67: 104277. doi: 10.1016/j.nanoen.2019.104277.

[24] Niu Simiao, Wang Sihong, Lin Long, et al. Theoretical study of contact-mode triboelectric nanogenerators as an effective power source[J]. Energy & Environmental Science, 2013, 6(12): 3576–3583. doi: 10.1039/C3EE42571A.